arXiv:2507.22787v2 [cond-mat.dis-nn] 12 Nov 2025

Amorphous Solid Model of Vectorial Hopfield Neural Networks

Filippo Gallavotti* and Alessio Zaccone†
Department of Physics "A. Pontremoli", University of Milan, via Celoria 16, 20133 Milan, Italy

We introduce a three-dimensional vectorial extension of the Hopfield associative-memory model in which each neuron is a unit vector on S^2 and synaptic couplings are 3×3 blocks generated through a vectorial Hebbian rule. The resulting block-structured operator is mathematically analogous to the Hessian of amorphous solids and induces a rigid energy landscape with deep minima for stored patterns. Simulations and spectral analysis demonstrate that the vectorial network substantially outperforms the classical binary Hopfield model: it exhibits a memory capacity that grows linearly with connectivity, a persistent spectral gap separating stored patterns from noise, and significantly enlarged basins of attraction. These results show that geometric constraints combined with amorphous-solid-inspired structure yield associative memories with markedly enhanced stability and retrieval performance.

The Hopfield model [1] has served as a cornerstone for understanding associative memory in neural networks and artificial intelligence. In its classical formulation, N binary neurons $s_i \in \{-1, +1\}$ evolve according to symmetric interactions W_{ij} defined by the Hebbian rules from stored patterns. The model's dynamics minimizes an energy function $E = -\frac{1}{2}\sum_{ij} W_{ij} s_i s_j$, leading to pattern retrieval through convergence to energy minima.

Recent developments have explored connections between neural network models and the physics of disordered materials, in particular spin glasses [2, 3] but also jammed packings [4, 5] and random resistor and memristive networks [6] and elastic networks [7]. In particular, recent work has been focused on understanding the close relationship between the "cost landscape" and the "physical landscape" as embodied by the cost Hessian matrix and the physical Hessian matrix, respectively [8].

The mathematical structure of neural networks shares fundamental similarities with amorphous solids, particularly in the organization of interaction matrices and the emergence of multiple metastable states. The Hessian matrix in amorphous solids, describing elastic interactions between particles, exhibits random block structure analogous to potential weight matrices in neural networks with vectorial degrees of freedom.

Motivated by this analogy, we introduce a multidimensional generalization of the Hopfield model. Each neuron is characterized by a unit vector $\mathbf{s}_i \in \mathbb{R}^3$, and interactions are constructed through outer products following a vectorial Hebbian rule. This approach leverages the concept of random block matrices previously introduced in the context of amorphous solids [9, 10] and only lately adopted in neural network theory [3].

The vectorial extension is not merely a mathematical generalization but reflects physical systems where orientational degrees of freedom play crucial roles, such as in liquid crystals, polymeric glasses, and biological networks (e.g. the cytoskeleton). Our approach reformulates the traditional Hopfield framework in terms of block-structured random matrices, enabling systematic comparison of learning efficiency and computational properties with classical binary models [11]. We shall start by reviewing the basic binary Hopfield model.

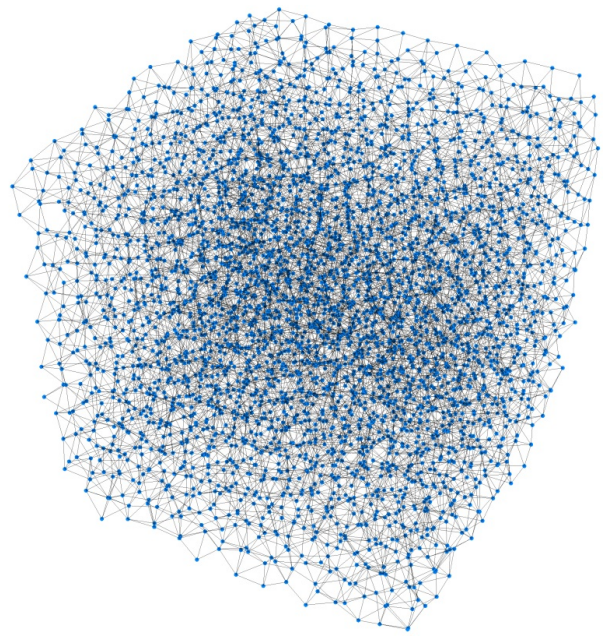

FIG. 1: Rendering of a 3D network of N nodes with an average coordination number $Z = 7$ and a fairly uniform distribution of orientation angles.

We consider 3D networks of N nodes (neurons) connected by 3D vectors ("bonds" or synapses) as depicted in Fig. 1. In the amorphous solid analogy, the connections between nodes are represented by springs with spring constant κ [12–14].

The binary Hopfield model consists of N neurons with states $s_i \in \{-1, +1\}$. To store P patterns $\{\boldsymbol{\xi}^\mu\}_{\mu=1}^P$ where $\boldsymbol{\xi}^\mu = (\xi_1^\mu, \ldots, \xi_N^\mu)$ with $\xi_i^\mu \in \{-1, +1\}$, the weight matrix is constructed using the Hebbian rule:

$$W_{ij} = \frac{1}{N}\sum_{\mu=1}^{P} \xi_i^\mu \xi_j^\mu \tag{1}$$

* filippo.gallavotti@studenti.unimi.it
† alessio.zaccone@unimi.it

with $W_{ii} = 0$ (no self-connections) and $W_{ij} = W_{ji}$ (symmetry).

The dynamics follows asynchronous updates: $s_i \leftarrow \text{sign}\left(\sum_j W_{ij} s_j\right)$, which minimizes the energy function $E = -\frac{1}{2}\sum_{ij} W_{ij} s_i s_j$. In words, this means that neuron i looks at the total input it receives from other neurons and updates its state accordingly, such that $\Delta E \leq 0$ is guaranteed. Pattern retrieval occurs when the system converges to stored configurations from partial or noisy initial states.

In the vectorial model, each neuron i is characterized by a unit vector $\mathbf{s}_i \in \mathbb{R}^3$ with $|\mathbf{s}_i| = 1$. We store P patterns $\{\boldsymbol{\xi}^\mu\}_{\mu=1}^P$, where each pattern consists of N random unit vectors uniformly distributed on S^2:

$$\boldsymbol{\xi}^\mu = (\boldsymbol{\xi}_1^\mu, \ldots, \boldsymbol{\xi}_N^\mu), \quad |\boldsymbol{\xi}_i^\mu| = 1. \tag{2}$$

The weight matrix is constructed through a vectorial Hebbian rule using outer products:

$$\mathbf{W}_{ij} = \frac{1}{N}\sum_{\mu=1}^{P} \boldsymbol{\xi}_i^\mu \otimes \boldsymbol{\xi}_j^\mu \tag{3}$$

where $\otimes$ denotes the outer product, yielding 3×3 matrices $\mathbf{W}_{ij}$ for each neuron pair ij. The global weight matrix $\mathbf{W}$ has dimensions $3N \times 3N$ with block structure [10].

This construction parallels the Hessian matrix in amorphous solids [9]. For elastic interactions between particles at positions $\mathbf{r}_i$, the Hessian elements are:

$$H_{ij}^{\alpha\beta} = \kappa_{ij} n_{ij}^\alpha n_{ij}^\beta \tag{4}$$

where κ_{ij} is the spring constant and $\mathbf{n}_{ij}$ is the unit vector along the bond direction, defined as:

$$\mathbf{n}_{ij} = (\sin\theta\cos\phi, \sin\theta\sin\phi, \cos\theta), \tag{5}$$

with $\alpha, \beta = \{x, y, z\}$. Again, self-interactions have been ignored. The mathematical structure is identical to Eq. (3), with stored patterns playing the role of sets of bond directions.

The energy function becomes:

$$E(\mathbf{s}) = -\frac{1}{2}\sum_{i,j=1}^{N} \mathbf{s}_i^T \mathbf{W}_{ij} \mathbf{s}_j \tag{6}$$

The dynamics preserves the unit vector constraint through normalization: each neuron receives a local field $\mathbf{h}_i = \sum_{j\neq i} \mathbf{W}_{ij}\mathbf{s}_j$ and updates according to $\mathbf{s}_i^{\text{new}} = \mathbf{h}_i/|\mathbf{h}_i|$.

As a first step, we verified that the vectorial Hopfield network correctly retrieves the stored memories. Starting from random initial configurations, the dynamics systematically converges to one of the memorized attractors or to their complementary states within a finite number of asynchronous updates. This behaviour demonstrates that the network is effectively able to stabilize the stored configurations as fixed points of the energy landscape, ensuring convergence within typically less than thirty update steps for all tested trials. The success of this retrieval test marks the first working implementation of the vectorial Hopfield model with three-dimensional neurons.

In order to construct the synaptic matrix responsible for such convergence, we employed the pseudo-inverse learning rule rather than the standard Hebbian one. The classical Hebbian prescription, infact, is known to perform optimally only when the stored patterns $\{\boldsymbol{\xi}^\mu\}$ are mutually orthogonal, a condition that rarely holds when P/N is finite. To overcome this limitation, we adopted a pseudo-inverse generalization that enforces exact retrieval of all stored configurations by construction. Defining the pattern matrix $\Xi = [\boldsymbol{\xi}^{(1)}\,\boldsymbol{\xi}^{(2)}\cdots\boldsymbol{\xi}^{(P)}]$ of size $3N \times P$, the Gram matrix of pattern overlaps is

$$G_{\mu\nu} = \frac{1}{N}\sum_{i=1}^{N} \boldsymbol{\xi}_i^\mu \cdot \boldsymbol{\xi}_i^\nu, \tag{7}$$

and its inverse G^{-1} allows one to define the pseudo-inverse operator

$$W = \frac{1}{N}\sum_{\mu,\nu=1}^{P} \Xi_\mu \, (G^{-1})_{\mu\nu} \, \Xi_\nu^\top, \tag{8}$$

which satisfies $W\Xi = \Xi$, i.e. every stored pattern becomes an exact eigenvector of W with eigenvalue 1. This guarantees perfect recall of all training patterns in the fully connected case. The use of the pseudo-inverse rule is thus essential to obtain a stable and exact retrieval even when patterns are correlated or non-orthogonal, and represents a natural extension of the classical formulation.

We then investigated how memory capacity depends on the degree of connectivity of the network. To this aim, we introduced a Z-connected topology, where each neuron is symmetrically coupled to its $Z/2$ nearest neighbours on either side along a circular ring. The coordination number Z thus measures the number of local links per neuron, interpolating between the fully connected ($Z = N-1$) and the sparse ($Z \ll N$) regimes. Mathematically, the adjacency matrix C_{ij} encodes these local connections and satisfies

$$C_{ij} = \begin{cases} 1, & \text{if } j \in \text{neigh}(i) \text{ or } i \in \text{neigh}(j), \\ 0, & \text{otherwise.} \end{cases}$$

The synaptic weights are then built locally by solving, for each neuron i, a regularized linear system that enforces the self-consistency condition between the target outputs $\boldsymbol{\xi}_i^\mu$ and the inputs from its neighbours $\boldsymbol{\xi}_j^\mu$ in all stored patterns. Denoting by $\mathcal{N}_i$ the set of neighbours of neuron i, the local weight matrices $\{W_{ij}\}_{j\in\mathcal{N}_i}$ are determined from

$$\sum_{j\in\mathcal{N}_i} W_{ij}\boldsymbol{\xi}_j^\mu \simeq \boldsymbol{\xi}_i^\mu, \qquad \forall\mu = 1, \ldots, P,$$

through a ridge-regularized least-squares solution of the form

$$W_i = (X_i X_i^\top + \lambda I)^{-1} X_i Y_i^\top,$$

where X_i is the matrix collecting neighbour states and Y_i contains the target states for neuron i. The parameter λ provides numerical stability and controls the effective smoothness of the local mapping. This local pseudo-inverse approach generalizes the fully connected rule to sparse graphs, preserving stability while encoding topological constraints in the learned operator.

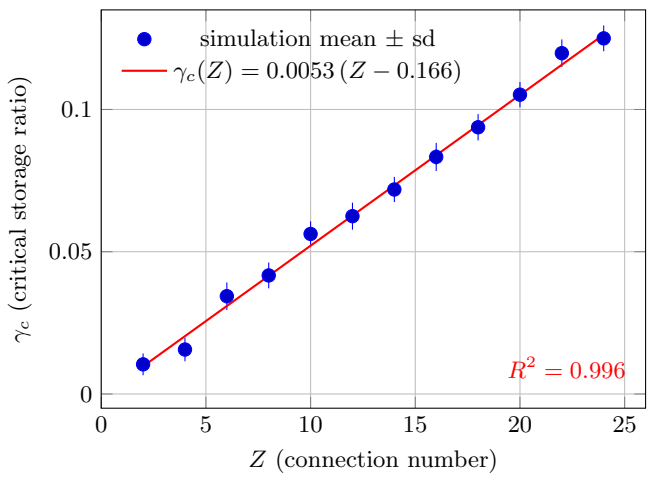

(a) Dynamical estimate

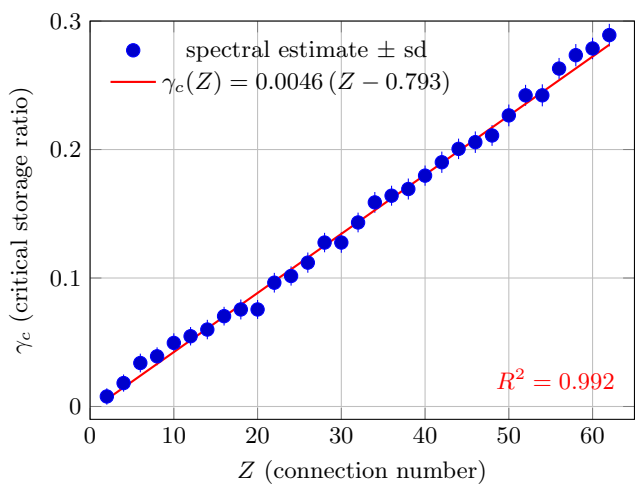

(b) Spectral estimate

FIG. 2: Critical storage capacity versus connectivity. (a) Bisection-based dynamical estimate with standard-deviation error bars across 5 replicas; (b) Spectral estimate from the vanishing smallest eigenvalue of the Hessian at each attractor. Both panels exhibit a linear dependence of γ_c on Z with closely matching slopes.

Figure 2 clearly shows that the critical storage capacity γ_c increases linearly with Z. A linear regression of the numerical data (performed over $N = 64$ neurons, $T = 500$ random trials, and $L = 1000$ maximum threshold of asynchronous updates) yields

$$\gamma_c(Z) = 0.0053\,(Z - 0.17), \qquad R^2 = 0.996.$$

This linear behaviour arises naturally from the additive contribution of independent local interactions to the overall stability of the stored patterns. Each additional connection per neuron reinforces the effective local field acting on every neuron, thereby enlarging the basins of attraction of the stored configurations. Increasing Z thus acts as a form of elastic stiffening of the associative energy landscape: the minima corresponding to memorized states become deeper and better separated as connectivity grows. The monotonic and nearly linear increase of γ_c with Z reflects a mean-field balance between the stabilizing role of recurrent couplings and the destabilizing effect of cross-talk among patterns.

To corroborate this interpretation, we performed a spectral analysis of the Hessian associated with each attractor, identifying γ_c as the point where the smallest eigenvalue $\lambda_{\min}$ vanishes. This criterion defines the loss of local stability of the attractor basin. The resulting relation, shown in Fig. 2b, reads

$$\gamma_c(Z) = 0.0046\,(Z - 0.79), \qquad R^2 = 0.992,$$

which is in excellent agreement with the direct dynamical estimate. The consistency between the dynamical and spectral approaches demonstrates that the transition from stable to unstable retrieval corresponds to a spectral softening of the Hessian, analogous to the vanishing of the lowest vibrational mode at the jamming transition. Hence, the linear dependence of γ_c on Z in both analyses supports the interpretation of associative-memory stability as an emergent rigidity phenomenon in a high-dimensional energy landscape.

We examine how pattern orientation distributions affect memory capacity by generating patterns using randomly distributed orientations for $\mathbf{n}_{ij}$. In particular, because the orientation of each unit vector $\mathbf{n}_{ij}$ is determined by a set of two angles $\{\theta, \phi\}$, cf. Eq. (5), both θ and ϕ are described, separately, by a Gaussian distribution normalized over the respective domains, i.e. $[0, \pi]$ for θ and $[0, 2\pi]$ for ϕ. In the limit of a completely uniform distribution $\sigma \to \infty$, the probability of a certain orientation in the solid angle is identically equal to $1/4\pi$ [9, 15].

We observed a critical coupling strength γ_c that shows a clear dependence on both the orientational disorder σ and network connectivity Z. As shown in Fig. 3, for each Z value, γ_c increases with σ, though the relationship is not strictly linear and shows some fluctuations due to the finite sampling of P_{critical}.

The data reveal a systematic hierarchy where networks with higher connectivity consistently achieve greater memory capacity. For $Z = 4$, γ_c ranges from 0.0104 to 0.0156, while for $Z = 16$, the capacity increases from 0.0313 to 0.0531 over the same σ range. This demonstrates that denser networks not only support higher

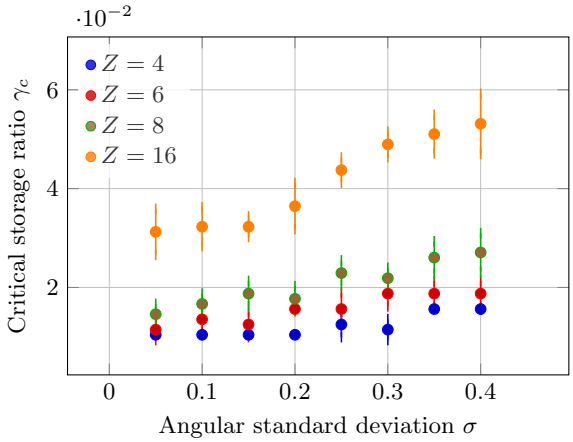

FIG. 3: Critical storage load $\gamma_c = P_c/(Nd)$ as a function of the angular standard deviation σ of the pattern-orientation distribution for different network connectivities Z. Higher connectivity networks exhibit greater memory capacity across all levels of orientational disorder, with all curves showing increasing γ_c with σ. Error bars represent standard deviation across 5 independent replicas.

baseline capacity but also benefit more significantly from orientational disorder.

The monotonic increase in γ_c with σ suggests that patterns with more diverse orientations create a more robust memory landscape, potentially by reducing interference between stored patterns through orientation-based differentiation. However, this enhanced stability comes at the cost of requiring stronger synaptic coupling, as evidenced by the higher γ_c values. The variations in the σ-γ_c relationship across different Z values indicate that network connectivity modulates how orientational disorder affects pattern stability, with highly connected networks showing greater sensitivity to orientation distribution changes.

Notably, for low connectivity ($Z = 4$), the capacity remains relatively constant at small σ values before increasing, whereas higher connectivity networks show more gradual and consistent growth with σ. This suggests that sparse networks require a minimum level of orientational diversity to overcome the limitations imposed by limited connectivity, while dense networks can leverage orientation diversity more effectively across the entire parameter range..

The vectorial Hopfield model creates energy landscapes with multiple local minima corresponding to stored patterns. We quantify the energy separation between stored configurations and random states to characterize pattern stability.

For system parameters $N = 25$ and $\gamma = 0.1$, stored patterns exhibit mean energies approximately 7 units lower than random configurations. This substantial energy gap ensures robust pattern retrieval against initialization noise. The energy function:

$$E(\mathbf{s}) = -\frac{1}{2}\sum_{i,j=1}^{N} \mathbf{s}_i^T \mathbf{W}_{ij} \mathbf{s}_j \tag{9}$$

naturally creates this hierarchical structure through the outer product construction of the weight matrix.

The energy gap magnitude scales inversely with pattern density, decreasing as γ approaches the critical threshold where memory capacity is lost. This behavior parallels metastable state hierarchies observed in glass-forming systems [16–18].

The eigenvalue spectrum of the weight matrix W_{ij} for the 3D networks proposed here, Eq. (1), provides information on computational properties at different pattern densities. With reference to Fig. 4 in the Appendix, we observe distinct spectral regimes, as follows.

For low pattern density ($\gamma = 0.05$), the spectrum is dominated by isolated eigenvalues corresponding to stored patterns, with the bulk distribution concentrated near zero. At intermediate pattern density ($\gamma = 0.1 - 0.2$), a spectral bulk emerges with pattern eigenvalues appearing as outliers. For high density ($\gamma = 0.5$), the spectrum transitions towards a random matrix behavior.

The spectral density evolution with γ reflects the crossover from a memory-dominated regime to a noise-dominated regime. The critical pattern density γ_c corresponds to the point where pattern eigenvalues merge with the spectral bulk, marking the loss of pattern discriminability.

The dynamics exhibits convergence behavior that depends critically on initialization and pattern density. We characterize basin properties through convergence statistics, as follows.

The convergence time scales logarithmically with the system size N for successful retrievals. The basin size decreases as γ approaches γ_c, following approximately exponential scaling. Near the memory capacity threshold, basins develop complex boundaries leading to sensitive dependence on initial conditions.

The unit vector normalization constraint creates dynamics on the product manifold $S^2 \times S^2 \times \cdots \times S^2$. This geometric constraint preserves pattern structure but introduces complexity compared to unconstrained dynamics. The update rule:

$$\mathbf{s}_i^{(t+1)} = \frac{\mathbf{h}_i^{(t)}}{|\mathbf{h}_i^{(t)}|}, \quad \mathbf{h}_i^{(t)} = \sum_{j \neq i} \mathbf{W}_{ij} \mathbf{s}_j^{(t)} \tag{10}$$

ensures convergence to fixed points while maintaining the spherical constraint.

The block-structured weight matrix $\mathbf{W}$ encodes orientational correlations through its 3×3 blocks $\mathbf{W}_{ij}$. We analyze correlation properties by examining (i) the Frobenius norm $|\mathbf{W}_{ij}|_F$, measuring interaction intensity, and (ii) the anisotropy ratio $\lambda_{\max}/\lambda_{\min}$ of $\mathbf{W}_{ij}^T\mathbf{W}_{ij}$, measuring directional bias.

For typical systems, we observe mean correlation strength $\langle|\mathbf{W}_{ij}|_F\rangle \approx 0.02$ and mean anisotropy ratio $\langle\lambda_{\max}/\lambda_{\min}\rangle \approx 15$. The high anisotropy ratios indicate strongly directional interactions, reflecting the vectorial nature of stored patterns.

This correlation structure creates emergent organization in the weight matrix, with enhanced correlations between blocks corresponding to pattern pairs with similar orientations.

The vectorial Hopfield model presented here extends associative memory beyond binary states by equipping each neuron with an orientation on S^2, leading naturally to a block-structured weight matrix analogous to the Hessian of disordered solids. This correspondence explains the rigid energy landscape and the emergence of well-separated minima associated with stored patterns. The model displays robust retrieval dynamics governed by monotonic energy descent under the spherical constraint.

A key finding is the superior performance of the vectorial network relative to the classical Hopfield model. The storage capacity increases linearly with the coordination number Z, yielding significantly larger critical loads than in the binary case. Spectral analysis reveals a persistent gap between pattern modes and the bulk even near saturation, in contrast with the rapid signal–noise mixing that limits the standard Hopfield model. Furthermore, the orientational degrees of freedom produce larger and more stable basins of attraction, enabling reliable retrieval from highly corrupted initial conditions.

These results highlight the potential of physically motivated network architectures—particularly those inspired by elasticity and amorphous solids—to achieve enhanced associative-memory performance. Extensions include nonlinear learning rules, sparse or hierarchical connectivities, and higher-dimensional vector manifolds. Overall, the vectorial Hopfield framework provides a compact, high-capacity, and dynamically robust associative memory that markedly outperforms its classical binary counterpart.

ACKNOWLEDGMENTS

AZ gratefully acknowledges funding from the US Army DEVCOM Army Research Office through contract nr. W911NF-22-2-0256 and from the European Union through Horizon Europe ERC Grant number: 101043968 "Multimech". In the making of this paper, we became aware of similar observations in a vectorial spin-glass model [3], that appeared shortly before this preprint.

APPENDIX

In Fig. 4, we show the eigenvalue distribution of the weight matrix W_{ij} for the 3D networks proposed in this paper. The eigenvalue spectrum is obtained by direct numerical diagonalization of the weight matrix, Eq. (1), constructed for our networks. In Fig. 5 we show the typical time evolution of the Lyapunov energy as a function of the number of updated steps, giving evidence of the monotonic convergence of the dynamics in the proposed neural network model.

[1] J. J. Hopfield, Proceedings of the National Academy of Sciences **79**, 2554 (1982), https://www.pnas.org/doi/pdf/10.1073/pnas.79.8.2554.
[2] D. J. Amit, H. Gutfreund, and H. Sompolinsky, Phys. Rev. A **32**, 1007 (1985).
[3] F. Nicoletti, F. D'Amico, and M. Negri, "Statistical mechanics of vector hopfield network near and above saturation," (2025), arXiv:2507.02586 [cond-mat.dis-nn].
[4] M. Geiger, S. Spigler, S. d'Ascoli, L. Sagun, M. Baity-Jesi, G. Biroli, and M. Wyart, Phys. Rev. E **100**, 012115 (2019).
[5] G. Zhang, D. J. Heeger, and S. Martiniani, "Contrastive self-supervised learning as neural manifold packing," (2025), arXiv:2506.13717 [cs.LG].
[6] S. G. Hu, Y. Liu, Z. Liu, T. P. Chen, J. J. Wang, Q. Yu, L. J. Deng, Y. Yin, and S. Hosaka, Nature Communications **6**, 7522 (2015).
[7] L. E. Altman, M. Stern, A. J. Liu, and D. J. Durian, Phys. Rev. Appl. **22**, 024053 (2024).
[8] M. Stern, M. Guzman, F. Martins, A. J. Liu, and V. Balasubramanian, Phys. Rev. Lett. **134**, 147402 (2025).
[9] A. Zaccone and E. Scossa-Romano, Physical Review B **83**, 184205 (2011).
[10] G. M. Cicuta, J. Krausser, R. Milkus, and A. Zaccone, Phys. Rev. E **97**, 032113 (2018).
[11] J. A. Hertz, A. S. Krogh, and R. G. Palmer, *Introduction to the Theory of Neural Computation*, Santa Fe Institute Studies in the Sciences of Complexity, Vol. 1 (Addison–Wesley, Reading, MA, 1991) p. 327.
[12] R. Milkus and A. Zaccone, Phys. Rev. B **93**, 094204 (2016).
[13] R. Milkus and A. Zaccone, Phys. Rev. E **95**, 023001 (2017).
[14] A. Zaccone, *Theory of Disordered Solids* (Springer, Cham, 2023).
[15] A. Zaccone, J. R. Blundell, and E. M. Terentjev, Phys. Rev. B **84**, 174119 (2011).
[16] G. Biroli and J. Kurchan, Phys. Rev. E **64**, 016101 (2001).
[17] D. Han, D. Wei, J. Yang, H.-L. Li, M.-Q. Jiang, Y.-J. Wang, L.-H. Dai, and A. Zaccone, Phys. Rev. B **101**, 014113 (2020).
[18] P. Charbonneau, J. Kurchan, G. Parisi, P. Urbani, and F. Zamponi, Nature Communications **5**, 3725 (2014).

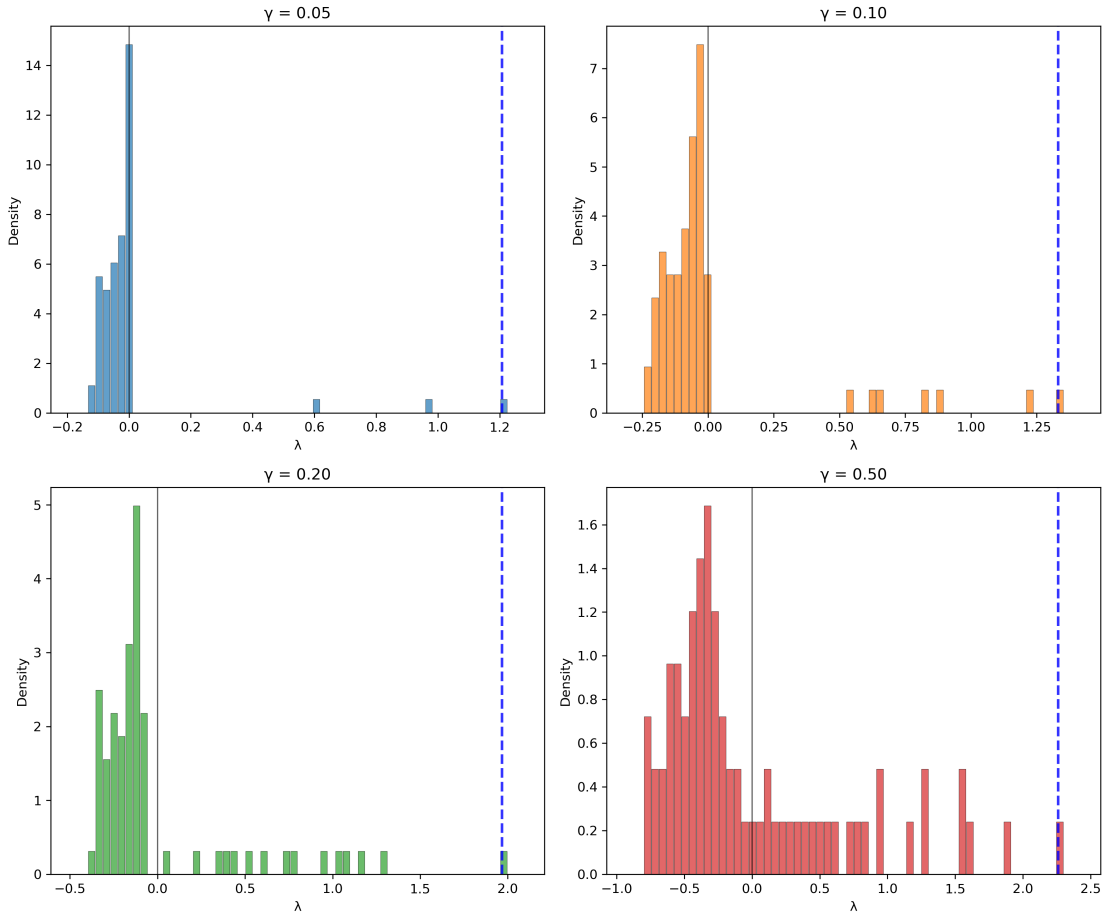

FIG. 4: Evolution of the spectral density $\rho(\lambda)$ of the weight matrix W_{ij} with different pattern capacities $\gamma = P/(Nd)$. Low density shows a concentrated band near zero with isolated positive eigenvalues, while high density exhibits broad continuous distributions, indicating pattern interference onset. The spectral density $\rho(\lambda)$ is obtained by direct numerical diagonalization of W_{ij}, as defined in Eq. (1), constructed for the 3D networks as in Fig. 1.

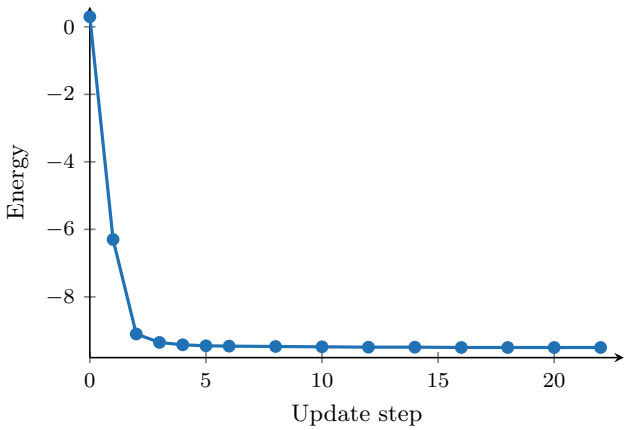

FIG. 5: Time evolution of the Lyapunov energy $E(t) = -\frac{1}{2}\,\mathbf{s}^\top W\,\mathbf{s}$ for a single synchronous run of the vector–Hopfield model with $N = 25$ neurons, $d = 3$, and $P = 5$ stored patterns. After a rapid decay in the first three updates the energy settles on the minimum corresponding to the retrieved pattern, confirming the monotonic convergence of the dynamics.